

OSTI^o
RC 3/12/92

AEROSPACE REPORT NO.
ATR 91(7171)-2

A Computer Modeling Study of Isotopically Selective, Laser Photodissociation of OCS in Cryogenic Solutions

Prepared by

PAUL F. ZITTEL
Space and Environment Technology Center
Technology Operations

23 December 1991

Prepared for

DEPARTMENT OF ENERGY
Washington, DC 20585

Grant No. DE-FG03-87ER13657

Engineering and Technology Group

THE AEROSPACE CORPORATION
El Segundo, California



PUBLIC RELEASE IS AUTHORIZED

DISTRIBUTION OF THIS DOCUMENT IS UNLIMITED

TECHNOLOGY OPERATIONS

The Aerospace Corporation functions as an "architect-engineer" for national security programs, specializing in advanced military space systems. The Corporation's Technology Operations supports the effective and timely development and operation of national security systems through scientific research and the application of advanced technology. Vital to the success of the Corporation is the technical staff's wide-ranging expertise and its ability to stay abreast of new technological developments and program support issues associated with rapidly evolving space systems. Contributing capabilities are provided by these individual Technology Centers:

Electronics Technology Center: Microelectronics, solid-state device physics, VLSI reliability, compound semiconductors, radiation hardening, data storage technologies, infrared detector devices and testing; electro-optics, quantum electronics, solid-state lasers, optical propagation and communications; cw and pulsed chemical laser development, optical resonators, beam control, atmospheric propagation, and laser effects and countermeasures; atomic frequency standards, applied laser spectroscopy, laser chemistry, laser optoelectronics, phase conjugation and coherent imaging, solar cell physics, battery electrochemistry, battery testing and evaluation.

Mechanics and Materials Technology Center: Evaluation and characterization of new materials: metals, alloys, ceramics, polymers and their composites, and new forms of carbon; development and analysis of thin films and deposition techniques; nondestructive evaluation, component failure analysis and reliability; fracture mechanics and stress corrosion; development and evaluation of hardened components; analysis and evaluation of materials at cryogenic and elevated temperatures; launch vehicle and reentry fluid mechanics, heat transfer and flight dynamics; chemical and electric propulsion; spacecraft structural mechanics, spacecraft survivability and vulnerability assessment; contamination, thermal and structural control; high temperature thermomechanics, gas kinetics and radiation; lubrication and surface phenomena.

Space and Environment Technology Center: Magnetospheric, auroral and cosmic ray physics, wave-particle interactions, magnetospheric plasma waves; atmospheric and ionospheric physics, density and composition of the upper atmosphere, remote sensing using atmospheric radiation; solar physics, infrared astronomy, infrared signature analysis; effects of solar activity, magnetic storms and nuclear explosions on the earth's atmosphere, ionosphere and magnetosphere; effects of electromagnetic and particulate radiations on space systems; space instrumentation; propellant chemistry, chemical dynamics, environmental chemistry, trace detection; atmospheric chemical reactions, atmospheric optics, light scattering, state-specific chemical reactions and radiative signatures of missile plumes, and sensor out-of-field-of-view rejection.

ATR--91(7171)2

DE92 009982

A COMPUTER MODELING STUDY OF ISOTOPICALLY SELECTIVE,
LASER PHOTODISSOCIATION OF OCS IN CRYOGENIC SOLUTIONS

Prepared by

Paul F. Zittel
Space and Environment Technology Center
Technology Operations

23 December 1991

Engineering and Technology Group
THE AEROSPACE CORPORATION
El Segundo, CA 90245-4691

Prepared for

DEPARTMENT OF ENERGY
Washington, DC 20585

Grant No. DE-FG03-87ER13657

PUBLIC RELEASE IS AUTHORIZED

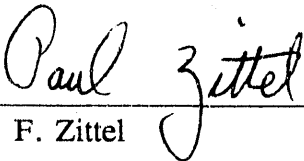
MASTER

ZFP

DISTRIBUTION OF THIS DOCUMENT IS UNLIMITED

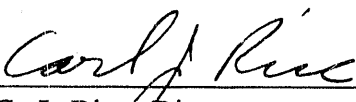
**A COMPUTER MODELING STUDY OF ISOTOPICALLY SELECTIVE,
LASER PHOTODISSOCIATION OF OCS IN CRYOGENIC SOLUTIONS**

Prepared

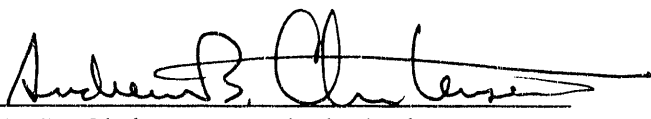


P. F. Zittel

Approved



C. J. Rice, Director
Target Signatures and Backgrounds
Department



A. B. Christensen, Principal Director
Space and Environment Technology Center

ABSTRACT

Computer model calculations are presented for enrichments of carbon, oxygen, and sulfur isotopes by two-step, IR/UV, laser photodissociation of OCS in rare gas liquid solutions. The model calculations are based on previously measured fundamental physical properties, including spectroscopic parameters of the IR absorption bands of OCS in cryogenic solution, UV photodissociation cross sections for specific vibrational levels of OCS, and rates for vibrational relaxation of OCS by cryogenic solvents. Results are presented for both pulsed and continuous wave laser sources. Photodissociation through both the $2\nu_2$ and ν_1 intermediate vibrational levels of OCS is investigated. The laser characteristics required to obtain optimum enrichments are determined by modeling the dependence of enrichment on laser wavelength and intensity, as well as pulse width and timing for pulsed sources. Optimum carbon and oxygen isotope enrichment factors of 9-14 are found for two-step photodissociation through the OCS($2\nu_2$) vibrational level, using pulsed CO₂ and KrF excimer laser sources. Optimum sulfur isotope enrichment factors of 5-6 are found for photodissociation through the OCS(ν_1) level, using a pulsed 12 μ m laser and a KrF excimer laser. The enrichments found for continuous wave laser sources are smaller than those for pulsed sources.

DISCLAIMER

This report was prepared as an account of work sponsored by an agency of the United States Government. Neither the United States Government nor any agency thereof, nor any of their employees, makes any warranty, express or implied, or assumes any legal liability or responsibility for the accuracy, completeness, or usefulness of any information, apparatus, product, or process disclosed, or represents that its use would not infringe privately owned rights. Reference herein to any specific commercial product, process, or service by trade name, trademark, manufacturer, or otherwise does not necessarily constitute or imply its endorsement, recommendation, or favoring by the United States Government or any agency thereof. The views and opinions of authors expressed herein do not necessarily state or reflect those of the United States Government or any agency thereof.

ACKNOWLEDGMENT

This work was supported by the Processes and Techniques Branch, Division of Chemical Sciences, Office of Basic Energy Sciences, Office of Energy Research, U.S. Department of Energy under Grant No. DE-FG03-87ER13657.

CONTENTS

ABSTRACT	v
ACKNOWLEDGMENT	vii
I. INTRODUCTION	1
II. KINETIC MODEL	3
III. COMPUTER MODELED ISOTOPE ENRICHMENTS	11
A. PULSED LASERS	11
1. Excitation in the OCS($2\nu_2$) Band	11
2. Excitation in the OCS(ν_1) Band	17
B. CONTINUOUS WAVE LASERS	23
IV. DISCUSSION	27
REFERENCES	29

FIGURES

1.	Isotopically Selective, Two-Step Photodissociation of OCS	3
2.	Pulsed Laser Parameters	11
3.	Dependence of Enrichment in Liquid Ar on CO ₂ Laser Line	12
4.	Dependence of Enrichment in Liquid Kr on CO ₂ Laser Line	13
5.	Dependence of Enrichment in Liquid Xe on CO ₂ Laser Line	14
6.	Dependence of Enrichment on Laser Pulse Widths and Delay	15
7.	Dependence of Enrichment on CO ₂ Laser Fluence	15
8.	Dependence of Enrichment on UV Laser Fluence	16
9.	Comparison of Experimental and Theoretical Enrichment Factors	17
10.	Dependence of Enrichment in Liquid Ar on 12 μm Laser Frequency	18
11.	Dependence of Enrichment in Liquid Kr on 12 μm Laser Frequency	18
12.	Dependence of Enrichment in Liquid Xe on 12 μm Laser Frequency	19
13.	Dependence of Sulfur Enrichment on Laser Pulse Widths and Delay	20
14.	Dependence of Enrichment on 12 μm Laser Fluence	20
15.	Dependence of Sulfur Enrichment on NH ₃ /KrF Laser Delay	22
16.	Dependence of Sulfur Enrichment on NH ₃ Laser Fluence	22
17.	Dependence of Enrichment on CW, CO ₂ Laser Intensity	24
18.	Dependence of Enrichment on CW, 12 μm Laser Intensity	24
19.	Schematic CW Laser Enrichment Apparatus	25

TABLES

1. $^{16}\text{O}^{12}\text{C}^{32}\text{S}$ Band Centers, Half-Widths, and Strengths in Cryogenic Solutions 5
2. Relative 249 nm Photodissociation Cross Sections of Vibrational Levels of OCS . . 6
3. OCS Vibrational Relaxation Times in Cryogenic Solutions 7
4. Estimated OCS($2\nu_2$) Relaxation Rate Constants in Cryogenic Solutions 9

I. INTRODUCTION

During the past several years, an experimental and computer modeling program in our laboratory has investigated the separation of stable isotopes by two-step laser photodissociation of OCS and other small molecules. The two-step enrichment method utilizes isotopically selective vibrational excitation of a molecule by an infrared laser, followed by ultraviolet laser photodissociation and chemical scavenging of the photofragments. Isotope enrichment in the photofragments occurs because of the large increase in the bound-continuous photodissociation cross section upon vibrational excitation. The program has experimentally demonstrated enrichments of carbon, oxygen and sulfur isotopes by two-step photodissociation of OCS. The experimental studies have considered isotope enrichment in the room temperature gas phase,¹⁻³ low temperature gas phase,⁴ and in cryogenic liquid solutions.^{5,6} The program has also investigated the fundamental physical processes of the two-step enrichment method. Of particular relevance to the present work are measurements of the spectra and vibrational relaxation rates of OCS dissolved in cryogenic liquids^{5,6} and measurements of photodissociation cross sections of specific, excited vibrational states of OCS.³

Two-step photodissociation of OCS in cryogenic solutions is a potentially efficient method of isotope separation because of the nature of the vibrational absorption bands of OCS in cryogenic solution, the relatively high solubility of OCS, and the simplicity of chemical scavenging of photogenerated sulfur atoms. Our previous studies have experimentally demonstrated oxygen isotope enrichment factors of 3-4 in rare gas liquid solutions;⁵ however, the enrichments fall short of what should be expected on the basis of measured photodissociation cross sections. The limiting factor in previous work was vibrational relaxation of OCS by the cryogenic solvent during the IR laser pumping process and the delay between IR and UV irradiation. Measurements of vibrational relaxation rates show that the relaxation processes occur on time scales of tens to hundreds of nanoseconds (ns),⁶ which are considerably shorter than the duration and jitter of the IR laser pulses currently available in our laboratory. The characteristics of these laser systems should not, however, be considered a fundamental limitation on the two-step enrichment process. Superior, short pulse, high power lasers are commercially available now. In addition, future developments in technology will produce electrically efficient, high power, wavelength tunable, infrared lasers, which will be ideally suited to the two-step enrichment method.

The fundamental photophysical information developed during the previous experimental studies provides a basis for modeling the enrichments that can be achieved with different laser sources. Experimental measurements of infrared spectral parameters in cryogenic solution, vibrationally state specific photodissociation cross sections, and vibrational relaxation rates in solution allow essentially *ab initio* modeling of two-step enrichment factors for arbitrary laser

characteristics. Some experimental studies of isotope enrichment conducted with less than ideal laser sources also provide points of comparison with computer modeled results.

This document reports a computer modeling study of carbon, oxygen, and sulfur isotope enrichment by two-step laser photodissociation of OCS in liquid Ar, Kr, and Xe. The study considers primarily pulsed IR and UV laser sources, although some discussion of continuous wave (cw) sources is included. The characteristics of the lasers (i.e., pulse duration, intensity, timing, etc.) are allowed to vary over wide ranges with the intent of defining the values necessary to achieve optimum isotope enrichment. Under favorable laser excitation conditions, the enrichments expected for each of the different rare isotopes of O, C, and S are investigated. This study deals exclusively with vibrational pumping of OCS in the $2\nu_2$ and ν_1 absorption bands since the required UV photodissociation cross sections and vibrational relaxation rates are known for these levels and levels of lower energy that would be populated by vibrational relaxation.

II. KINETIC MODEL

The kinetic model for the isotopically selective, two-step, laser photodissociation of OCS is summarized schematically in Fig. 1. OCS molecules are vibrationally excited with isotopic selectivity by an infrared laser in either the $2\nu_2$ vibrational band centered at a wavelength of $\sim 9.6 \mu\text{m}$, or in the ν_1 band centered at $\sim 11.6 \mu\text{m}$. For excitation in the $2\nu_2$ band, the modeling calculations are done for excitation by P-branch emission lines of the CO_2 laser, which

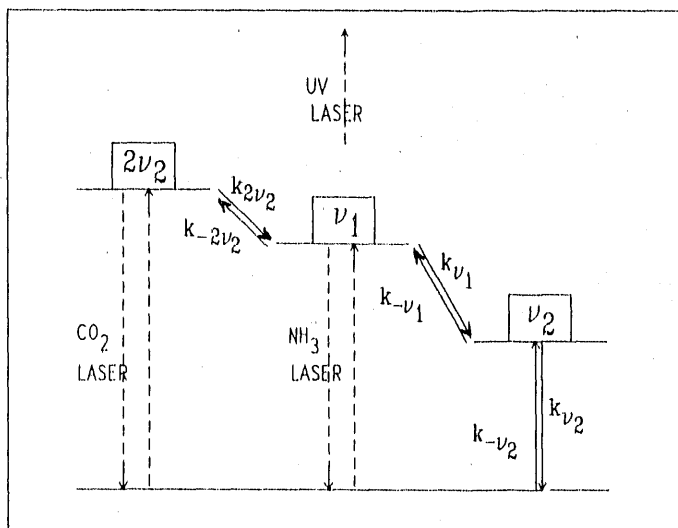


Figure 1. Isotopically Selective, Two-Step Photodissociation of OCS.

span the wavelength region of interest. For excitation in the ν_1 band, calculations are generally done as a function of emission wavelength for a hypothetical, tunable "12 μm laser". Some calculations are also done for specific emission lines of a real NH_3 molecular laser, which emits in the region of the $\text{OCS}(\nu_1)$ absorption band. Following vibrational excitation, the OCS molecules are irradiated and photodissociated by an ultraviolet, KrF excimer laser at a wavelength of 249 nm. The UV photodissociation cross section of OCS increases significantly with vibrational excitation, resulting in isotopic enrichment in the photodissociation products. It is assumed (and verified by experiment⁵) that the isotopic selectivity achieved by the two-step photodissociation process can be completely maintained during subsequent chemical scavenging of the CO and S atom products. Sulfur atoms are recombined to form solid sulfur particulate in rare gas liquid solutions, or are converted to SO_2 in solutions containing dissolved oxygen at levels of $\sim 1\%$. A critical factor during the two-step photodissociation process is the vibrational relaxation of the IR laser-pumped OCS molecules *by the cryogenic solvent*. In these modeling calculations OCS concentrations of ~ 1 part per million (ppm) are assumed so that vibrational relaxation of OCS by itself, or transfer of vibrational excitation among different isotopomers of

OCS, can generally be neglected even if it occurs with unit collision efficiency. Since energy transfer among OCS isotopomers is negligible, it is possible to treat the photodissociation of each isotopomer separately, using the appropriate, isotopically dependent, IR photoabsorption cross sections.

The infrared spectra of OCS dissolved in cryogenic rare gas liquids have been investigated in detail in our laboratory.^{5,6} A vibrational absorption band, which consists of 50-60 significant rotational lines in the gas phase, is collapsed to a single, intense feature in cryogenic solution. The cryogenic bands are Lorentzian in shape and are presumably homogeneously broadened. The IR absorption cross section at wavenumber $\bar{\nu}$ is given by Eq. (1),

$$\sigma_{IR}(\bar{\nu}) = \frac{S}{\pi} \frac{\gamma}{(\bar{\nu} - \bar{\nu}_0)^2 + \gamma^2} \quad (1)$$

where S is the integrated band strength, $\bar{\nu}_0$ is the band center, and γ is the band half-width at half-maximum (hwhm). The relevant spectroscopic parameters for the $^{16}\text{O}^{12}\text{C}^{32}\text{S}$ isotopomer are reproduced in Table 1. The band centers of other isotopomers $^x\text{O}^y\text{C}^z\text{S}$ are generally calculated from Eq. (2), using the well known gas phase band centers of the isotopomers,

$$\bar{\nu}_0(^x\text{O}^y\text{C}^z\text{S})_{\text{liquid}} = \frac{\bar{\nu}_0(^{16}\text{O}^{12}\text{C}^{32}\text{S})_{\text{liquid}}}{\bar{\nu}_0(^{16}\text{O}^{12}\text{C}^{32}\text{S})_{\text{gas}}} \bar{\nu}_0(^x\text{O}^y\text{C}^z\text{S})_{\text{gas}} \quad (2)$$

The isotopomer band centers calculated from Eq. (2) are in excellent agreement with band centers measured in liquid Ar solution.⁵ For the $^{17}\text{O}^{12}\text{C}^{32}\text{S}$ isotopomer, the gas phase band centers are not known; however, the band centers in liquid Ar have been measured,⁵ and the band centers in liquid Kr and Xe are derived from the relationship implicit in Eq. (2). It is assumed that the band half-widths are the same for the different isotopomers. An expected small dependence of band strength on the different vibrational masses of the isotopomers is neglected. The stimulated emission cross section σ_{-IR} for the reverse of the IR absorption process is taken to be equal to the absorption cross section multiplied by the ratio of the vibrational degeneracy of the lower level of the transition to the degeneracy of the upper level (i.e., $\sigma_{-IR} = \sigma_{IR} d_l/d_u$). Thus, it is assumed that relaxation among the different vibrational angular momentum sublevels of a "degenerate" vibrational level is extremely rapid.

The UV photodissociation cross section of OCS is a strong function of vibrational level. The relative photodissociation cross sections at the KrF excimer laser wavelength of 249 nm have been measured experimentally³ in the gas phase for the relevant vibrational levels of OCS and are reproduced in Table 2. It is assumed that the relative cross sections are essentially the same in cryogenic liquid solution. In these modeling calculations, the UV laser fluence (i.e.,

Table 1. $^{16}\text{O}^{12}\text{C}^{32}\text{S}$ Band Centers, Half-Widths, and Strengths in Cryogenic Solutions. ^{a,b}

	upper vibrational level ^c		
	(01 ¹ 0)	(10 ⁰ 0)	(02 ⁰ 0)
	$\bar{\nu}_0, \text{cm}^{-1}$		
Ar(l)	519.77	858.93	1045.42
Kr(l)	518.73	858.42	1043.42
Xe(l)	517.18	857.69	1040.40
O ₂ (l)	520.01	859.14	1045.88
gas ^d	520.42	858.97	1047.04
	γ, cm^{-1}		
Ar(l)	0.34	0.65	0.71
Kr(l)	0.40	0.80	0.82
Xe(l)	0.63	1.14	1.32
O ₂ (l)	0.36	0.67	0.76
	$S, ^e 10^{-19} \text{ cm/molecule}$		
Ar(l)	7.0	12.0	4.8
Kr(l)	7.0	12.0	4.8
Xe(l)	6.7	10.5	4.6
O ₂ (l)	7.5	12.6	4.9
gas ^d	4.8	14.7	4.8

^a Data for cryogenic solutions are from Refs. 5 and 6.

^b Temperatures of Ar, Kr, Xe and O₂ solutions are 84.4, 116.8, 162.0 and 78.6 K, respectively.

^c Lower vibrational level is (00⁰0).

^d Literature citations for the OCS gas phase band centers and strengths are compiled in Ref 5.

^e Band strengths are corrected to 100% $^{16}\text{O}^{12}\text{C}^{32}\text{S}$.

time-integrated intensity) is generally taken to be much smaller than the fluence required to saturate the photodissociation from any of the vibrational levels. In some cases the effect of increasing the UV fluence to the saturation level is investigated. In modeling actual experimental results, the true experimental UV laser fluences are used. The modeling calculations are restricted to a UV wavelength of 249 nm since the photodissociation cross sections from specific, vibrationally excited levels of OCS have not been measured at other wavelengths. The ratio of the photodissociation cross section for a particular excited vibrational

Table 2. Relative 249 nm Photodissociation Cross Sections of Vibrational Levels of OCS.^a

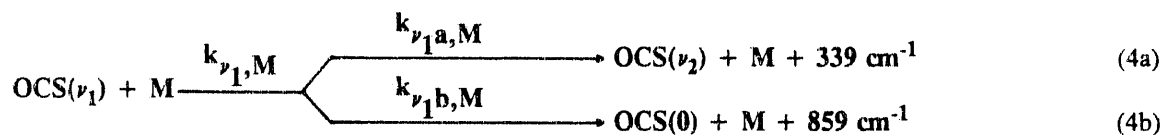
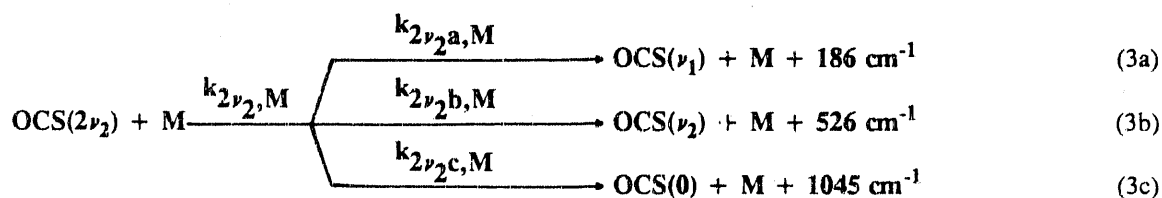
i	$\sigma_{UV,i}/\sigma_{UV,0}^b$
ν_2	6.2 ± 1.9
ν_1	11.0 ± 3.4
$2\nu_2$	20.5 ± 4.6

^a From Ref. 3.

^b Cross sections are relative to the cross section of the ground vibrational level, which is taken to be $\sigma_{UV,0} = 5.70 \times 10^{-21} \text{ cm}^2/\text{molecule}$. See Ref. 3.

level to the cross section for the ground level is in theory a strong function of UV wavelength, becoming larger with increasing wavelength as the energy threshold for the photodissociation process is approached. At longer UV wavelengths, larger enrichment factors and somewhat smaller product yields per laser shot would generally be expected.

A critical factor in determining the isotope enrichment achieved by the two-step photodissociation process is the effect of vibrational relaxation of the IR laser-pumped OCS molecules. The relaxation processes relevant to the present modeling study are summarized in Eqs. (3)-(5),



where the exothermicities are given for $^{16}\text{O}^{12}\text{C}^{32}\text{S}$ in liquid Ar. The total relaxation rate constants $k_{\nu_1,\text{M}}$ and $k_{\nu_2,\text{M}}$ have been measured experimentally in our laboratory⁶ for various

cryogenic solvents M, and a lower limit has been placed on $k_{2\nu_2, M}$. The experimental results are reproduced in Table 3 along with a theoretical estimate of $k_{2\nu_2, M}$, which is described below. The branching ratios for the multiple paths possible in the relaxation of the $2\nu_2$ and ν_1 levels are not known. Theory predicts a strong negative dependence of relaxation probability on exothermicity. The dependence becomes very strong as the exothermicities become larger than kT , where T is the temperature of the sample. For the cryogenic conditions of the previous

Table 3. OCS Vibrational Relaxation Times in Cryogenic Solutions.

vibr level	solvent	T	$\tau_{i, M}$	$k_{i, M}^a$	$P_{IBC, hs}^b$
i	M	(K)	(ns)	($10^{-16} \text{ cm}^3/\text{s}$)	
$2\nu_2^c$	Ar	84.4	9	52	8.5×10^{-6}
	Kr	116.8	17	34	6.0×10^{-6}
	Xe	162.0	6	120	1.2×10^{-5}
	O ₂	84.4	-	-	-
ν_1^d	Ar	84.4	145 \pm $\begin{smallmatrix} 35 \\ 40 \end{smallmatrix}$	3.3 \pm $\begin{smallmatrix} 1.2 \\ 0.7 \end{smallmatrix}$	5.3 \pm $\begin{smallmatrix} 2.0 \\ 1.1 \end{smallmatrix} \times 10^{-7}$
	Kr	116.8	235 \pm $\begin{smallmatrix} 60 \\ 65 \end{smallmatrix}$	2.4 \pm $\begin{smallmatrix} 1.0 \\ 0.5 \end{smallmatrix}$	4.3 \pm $\begin{smallmatrix} 1.7 \\ 0.8 \end{smallmatrix} \times 10^{-7}$
	Xe	162.0	250 \pm $\begin{smallmatrix} 150 \\ 95 \end{smallmatrix}$	2.8 \pm $\begin{smallmatrix} 1.6 \\ 1.1 \end{smallmatrix}$	2.9 \pm $\begin{smallmatrix} 1.8 \\ 1.1 \end{smallmatrix} \times 10^{-7}$
	O ₂ ^e	84.4	22 \pm $\begin{smallmatrix} 8 \\ 7 \end{smallmatrix}$	21. \pm $\begin{smallmatrix} 9 \\ 8 \end{smallmatrix}$	2.6 \pm $\begin{smallmatrix} 1.1 \\ 0.7 \end{smallmatrix} \times 10^{-6}$
ν_2^d	Ar	84.4	355 \pm 35	1.33 \pm 0.13	2.2 \pm 0.2 $\times 10^{-7}$
	Kr	116.8	660 \pm 60	0.87 \pm 0.08	1.6 \pm 0.2 $\times 10^{-7}$
	Xe	162.0	625 \pm 75	1.10 \pm 0.13	1.2 \pm 0.1 $\times 10^{-7}$
	O ₂ ^e	84.4	53 \pm 9	8.6 \pm 1.5	1.1 \pm 0.2 $\times 10^{-6}$

^a $k_{i, M} = 1/\tau_{i, M} N_M$, where N_M is the solvent density calculated to be 2.12, 1.75, 1.45 and $2.20 \times 10^{22}/\text{cm}^3$ for liquid Ar, Kr, Xe and O₂, respectively, at the stated temperatures.

^b $P_{IBC, hs} = k_{i, M} N_M / K_{hs, M}$, where $K_{hs, M}$ is the hard sphere collision rate calculated to be 1.31, 0.98, 1.36 and $1.78 \times 10^{13} \text{ s}^{-1}$ for OCS dilute in liquid Ar, Kr, Xe and O₂, respectively, at the stated temperatures.

^c Relaxation rate constants for $2\nu_2$ level are estimated from isolated binary collision theory and experimental room temperature, gas phase data from Ref. 7. Details of the estimate appear in Table 4. An upper limit of 70 ns was determined experimentally for $\tau_{2\nu_2, M}$ in Ref. 6 for all four cryogenic solvents.

^d Experimental relaxation rate constants for ν_1 and ν_2 levels are from Ref. 6.

^e Measured in O₂/Ar liquid mixtures and extrapolated to 100% O₂(l).

rate constant measurements and the present modeling study, it is reasonable to assume that a total relaxation rate constant is essentially equal to the rate constant for the path of least exothermicity, and that other relaxation paths are negligible by comparison. Therefore, the assumptions used in this modeling study are $k_{2\nu_2a,M} = k_{2\nu_2,M}$, $k_{\nu_1a,M} = k_{\nu_1,M}$, and $k_{2\nu_2b,M} = k_{2\nu_2c,M} = k_{\nu_1b,M} = 0$. In discussing the modeling study, it is often convenient to consider a *relaxation rate*, which is equal to the product of a rate constant and a solvent number density (i.e., $K_{i,M} = k_{i,M}N_M$), or a *relaxation time*, which is the reciprocal of a relaxation rate (i.e., $\tau_{i,M} = 1/K_{i,M}$). Even at cryogenic temperatures, it is necessary to include the reverse endothermic relaxation processes in the kinetic model (Fig. 1). The reverse rates $K_{-i,M}$ are obtained from the forward rates by detailed balance.

Since only lower limits on the rate constants for relaxation of the OCS($2\nu_2$) vibrational level have been determined experimentally, a theoretical extrapolation procedure has been used to estimate the cryogenic rate constants from experimentally measured,⁷ room temperature, gas phase data. The extrapolation is based on the isolated binary collision theory of liquid phase encounters and on vibrational energy transfer theory. The approach has been described in detail and applied to OCS and O₃ in cryogenic solutions in a previous paper.⁶ The extrapolation determines the ratio of the relaxation rate constant in the liquid phase at temperature T_{liq} to the rate constant in the room temperature gas phase at temperature T_{gas} from Eq. (6),

$$\frac{k_{liq}(T_{liq})}{k_{gas}(T_{gas})} = \frac{g_{hs}(\sigma)}{\exp(\epsilon/kT_{gas})} \left(\frac{T_{liq}}{T_{gas}} \right)^{1/2} \frac{\langle P_{gas}(T_{liq}) \rangle}{\langle P_{gas}(T_{gas}) \rangle} \quad (6)$$

where σ and ϵ are Lennard-Jones intermolecular potential parameters for the OCS/solvent collision, and $\langle P_{gas}(T) \rangle$ is a relaxation probability per collision calculated from energy transfer theory for gas phase encounters at temperature T . The term $g_{hs}(\sigma)$ is a hard sphere, radial pair distribution function and is roughly the factor by which binary collision rate constants are increased in the liquid phase relative to the low pressure gas phase because of the finite volumes of atoms and molecules. The ratio of gas phase relaxation probabilities in the final term of Eq. (6) was calculated for the process in Eq. (3a), using first order distorted wave theory for an exponentially repulsive potential and also for a Morse intermolecular potential. Both model potentials were derived from the same Lennard-Jones potential parameters for OCS/solvent collisions. The results of the extrapolation procedure are summarized in Table 4. The extrapolated rate constants are equivalent to relaxation times of 9, 17, and 6 ns for relaxation of OCS($2\nu_2$) by liquid Ar, Kr, and Xe, respectively. The uncertainties in the experimentally measured gas phase rate constants used in the extrapolation and the approximate nature of the theoretical extrapolation procedure do not support a confidence level of better than a factor of 2 in the estimated relaxation rate constants for OCS($2\nu_2$). In order to minimize complexity, a $2\nu_2$ relaxation time of 10 ns has been used in all modeling calculations for all solvents, unless

Table 4. Estimated OCS($2\nu_2$) Relaxation Rate Constants in Cryogenic Solutions.

M	$k_{\text{gas}}(T_{\text{gas}})^a$ (cm^3/s)	$g_{\text{hs}}(\sigma)$	$\frac{\langle P_{\text{gas}}(T_{\text{liq}}) \rangle}{\langle P_{\text{gas}}(T_{\text{gas}}) \rangle}^b$		$k_{\text{liq}}(T_{\text{liq}})^c$ (cm^3/s)
			EXP REP ^d	MORSE ^e	
Ar	$2.8 \pm 0.9 \times 10^{-14}$	5.02	0.18	0.08	5.2×10^{-15}
Kr	$1.5 \pm 0.3 \times 10^{-14}$	4.46	0.23	0.11	3.4×10^{-15}
Xe	$2.2 \pm 0.3 \times 10^{-14}$	6.19	0.33	0.21	1.2×10^{-14}

^a Measured in the gas phase at $T_{\text{gas}} = 300\text{K}$. From Ref. 7.

^b Calculated from energy transfer theory for gas phase binary collisions. See Ref. 6.

^c Calculated from Eq. (6), using the average of the two theoretical values for $\langle P_{\text{gas}}(T_{\text{liq}}) \rangle / \langle P_{\text{gas}}(T_{\text{gas}}) \rangle$.

^d Calculated for an exponentially repulsive intermolecular potential.

^e Calculated for a Morse intermolecular potential.

otherwise noted.

For IR laser excitation in the $0 \rightarrow 2\nu_2$ vibrational band, the kinetic equations that describe the populations in the four relevant vibrational levels of a particular isotopomer of OCS during the two-step photodissociation process are summarized by the matrix equation,

$$\begin{pmatrix} \dot{n}_{2\nu_2} \\ \dot{n}_{\nu_1} \\ \dot{n}_{\nu_2} \\ \dot{n}_0 \end{pmatrix} = \begin{pmatrix} -K_{2\nu_2} - I_{\text{IR}}\sigma_{\text{-IR}} - I_{\text{UV}}\sigma_{\text{UV},2\nu_2} & K_{-2\nu_2} & 0 & I_{\text{IR}}\sigma_{\text{IR}} \\ K_{2\nu_2} & -K_{\nu_1} - K_{-2\nu_2} - I_{\text{UV}}\sigma_{\text{UV},\nu_1} & K_{-\nu_1} & 0 \\ 0 & K_{\nu_1} & -K_{\nu_2} - K_{-\nu_1} - I_{\text{UV}}\sigma_{\text{UV},\nu_2} & K_{-\nu_2} \\ I_{\text{IR}}\sigma_{\text{-IR}} & 0 & K_{\nu_2} & -K_{-\nu_2} - I_{\text{IR}}\sigma_{\text{IR}} - I_{\text{UV}}\sigma_{\text{UV},0} \end{pmatrix} \begin{pmatrix} n_{2\nu_2} \\ n_{\nu_1} \\ n_{\nu_2} \\ n_0 \end{pmatrix} \quad (7)$$

An analogous equation with the appropriate IR absorption terms applies to pumping in the $0 \rightarrow \nu_1$ band. The variable n_i is the number density of molecules of the particular isotopomer in vibrational level i . The terms I_{IR} and I_{UV} are, respectively, the time dependent infrared and ultraviolet laser intensities expressed in photons/ cm^2/sec . The IR absorption/emission cross sections are specific to the particular isotopomer under consideration. The four coupled differential equations implied by Eq. (7) are integrated numerically through the laser irradiation

process starting with the initial vibrational populations at thermodynamic equilibrium. For the case of cw laser irradiation, Eq. (7) can also be solved analytically by matrix inversion methods. Since energy transfer between different isotopomers can be made negligible at small OCS concentrations, Eq. (7) is solved separately for each OCS isotopomer. The initial sample consists of the most abundant isotopomer $^{16}\text{O}^{12}\text{C}^{32}\text{S}$ (93.72%) and the singly substituted isotopomers, $^{17}\text{O}^{12}\text{C}^{32}\text{S}$ (0.04%), $^{18}\text{O}^{12}\text{C}^{32}\text{S}$ (0.19%), $^{16}\text{O}^{13}\text{C}^{32}\text{S}$ (1.05%), $^{16}\text{O}^{12}\text{C}^{33}\text{S}$ (0.75%), and $^{16}\text{O}^{12}\text{C}^{34}\text{S}$ (4.16%) at the natural abundances noted in parentheses. The remaining isotopomers (0.09%), which involve the very rare ^{36}S isotope and multiply-substituted isotopomers, are ignored. After the conclusion of the UV laser pulse, the surviving populations in the four vibrational levels of a particular isotopomer are summed and compared with the original total population of the isotopomer to determine the amount of photodissociation. The abundance of a particular atomic isotope in the photodissociation products is then obtained by summing the photodissociated number density over all isotopomers that contain the atomic isotope.

The results of the modeling calculations are generally expressed as isotope enrichment factors. The enrichment of atomic isotope x with respect to isotope y in the photodissociation products is defined by Eq. (8),

$$\beta_y^0(x) = \frac{([x]/[y])_{\text{product}}}{([x]/[y])_{\text{original}}} \quad (8)$$

where "product" indicates isotopic abundance in the photodissociation products and "original" indicates isotopic abundance in the original OCS prior to any photodissociation. The enrichment factors modeled in this study are the result of a single IR/UV laser shot, indicated in Eq. (8) by the superscript zero. In those cases where modeled enrichments are compared with experimental results, the experimental enrichment factors, which are typically the result of many laser shots, are corrected to single-shot enrichments by a straightforward procedure.⁵

III. COMPUTER MODELED ISOTOPE ENRICHMENTS

A. PULSED LASERS

1. Excitation in the OCS($2\nu_2$) Band

For most of the modeling calculations for pulsed lasers in this study, the laser intensities are assumed to be Gaussian in time dependence and are described by Eq. (9),

$$I_{IR}(t) = \frac{F_{IR} (\ln 2)^{1/2}}{\pi^{1/2} \gamma_{IR}} \exp[-\ln 2 (t / \gamma_{IR})^2]$$

$$I_{UV}(t) = \frac{F_{UV} (\ln 2)^{1/2}}{\pi^{1/2} \gamma_{UV}} \exp[-\ln 2 ((t - \delta_{IR/UV}) / \gamma_{UV})^2]$$

for $t \geq -\infty$

(9)

where F_{IR} and F_{UV} are, respectively, the infrared and ultraviolet laser fluences in photons/cm², γ_{IR} and γ_{UV} are the pulse half-widths at half-maximum, and $\delta_{IR/UV}$ is the delay between the maxima in the IR and UV intensities. The laser parameters are illustrated schematically in Fig.

2. Variations from the general functional form in the case of specific experimental laser sources, or cw lasers, are noted as necessary.

The laser parameters are varied over wide ranges to investigate the effects of laser tuning, vibrational relaxation, absorption saturation, and other factors on isotope enrichments.

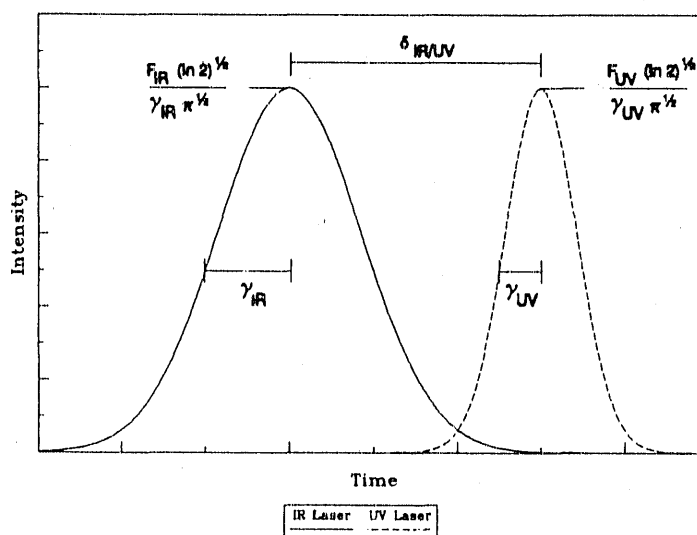


Figure 2. Pulsed Laser Parameters.

In many cases, nominal values of 0.75 J/cm^2 and 0.2 J/cm^2 are used for the IR and UV laser fluences, respectively. The nominal IR laser fluence corresponds to approximately 4-8 times the fluence necessary to saturate the absorption at the *center* of the $2\nu_2$ vibrational band (i.e., $\sim \pi\gamma/S$ photons/cm²). The nominal UV fluence is a factor of ~ 35 smaller than the fluence necessary to saturate photodissociation out of the vibrational level with the largest UV cross section (i.e., $\sim 1/\sigma_{\text{UV},2\nu_2}$ photons/cm²). Thus, parametric studies with the nominal IR and UV laser fluences investigate enrichments for the case where the isotopically selective IR absorption process is pumped hard to achieve high selectivity, and the UV photodissociation process is pumped weakly in order to non-intrusively sample the IR-induced isotopic selectivity. In many cases, nominal laser pulse full-widths and an IR/UV delay of 1 ns are used. A characteristic two-step photodissociation time of 1 ns is an order of magnitude shorter than the fastest vibrational relaxation time in the system (i.e., $\tau_{2\nu_2, M}$). Thus, parametric studies with the nominal laser pulse widths and delay investigate enrichment essentially in the absence of vibrational relaxation.

The isotope enrichment factors calculated in liquid Ar solution with different CO₂ laser excitation lines are shown in Fig. 3 for nominal laser fluences, pulse widths, and delay. In Fig. 3 and subsequent figures, the legend notation "x/y" indicates the enrichment of atomic isotope x with respect to atomic isotope y (e.g., "18/16" indicates the oxygen isotope enrichment factor $\beta_{16}^0(18)$). All modeled enrichments are for a single laser shot. For the laser conditions of Fig.

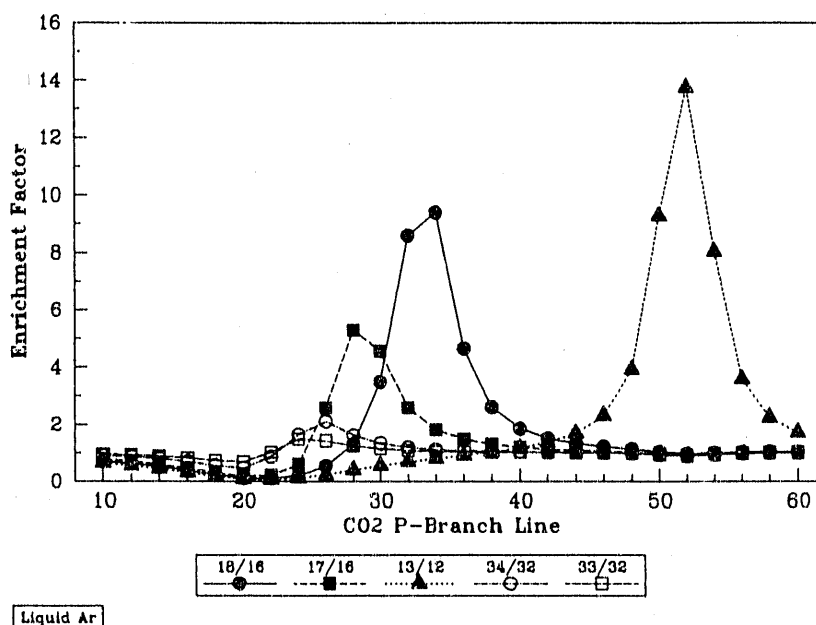


Figure 3. Dependence of Enrichment in Liquid Ar on CO₂ Laser Line. $F_{\text{IR}}=0.75 \text{ J/cm}^2$; $F_{\text{UV}}=0.2 \text{ J/cm}^2$; $2\gamma_{\text{IR}}=2\gamma_{\text{UV}}=\delta_{\text{IR/UV}}=1 \text{ ns}$.

3, the effects of vibrational relaxation are negligible. The theoretical maximum enrichment factor for the two-level system involving only the optically connected $2\nu_2$ and ground vibrational levels with perfectly resolved isotopic bands and no vibrational relaxation is given by Eq. (10),

$$\beta_y^0(x)_{\max} = \frac{d_{2\nu_2}}{d_{2\nu_2} + d_0} \left(\frac{\sigma_{UV,2\nu_2}}{\sigma_{UV,0}} - 1 \right) + 1 \quad (10)$$

where d_i is the vibrational degeneracy of level i , and $\sigma_{UV,i}$ is the photodissociation cross section. The enrichment of ^{13}C with respect to ^{12}C is close to the theoretical maximum of ~ 15.6 calculated from Eq. (10). The large enrichment factor is realized because of the large isotope shift in the $2\nu_2$ absorption band center relative to the bandwidth upon ^{13}C isotopic substitution. Smaller enrichments are found for oxygen isotopes due to smaller isotopic shifts and consequently greater overlapping of the IR absorption bands. Sulfur enrichments are very small because of the very small shifts in the $2\nu_2$ band center upon sulfur isotopic substitution. Figures 4 and 5 show analogous results for liquid Kr and Xe solutions, respectively.

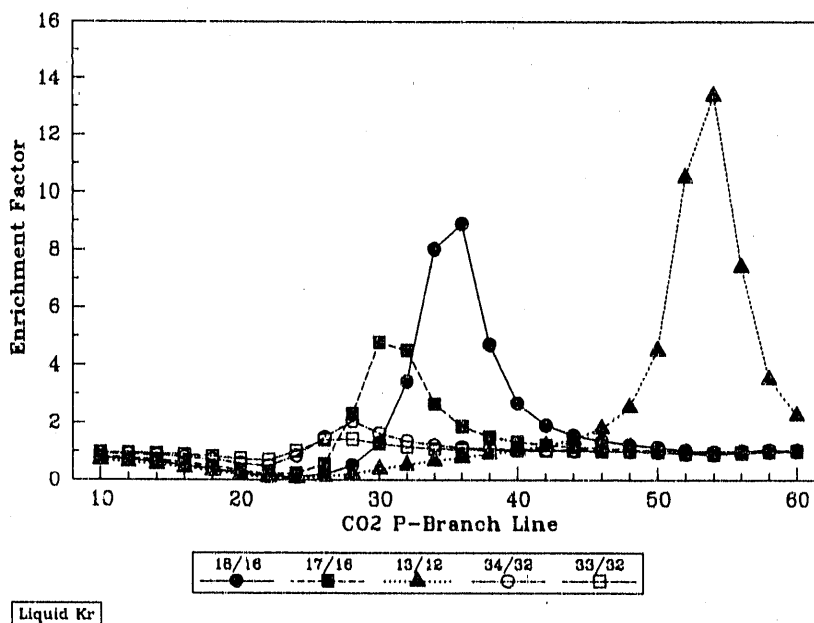


Figure 4. Dependence of Enrichment in Liquid Kr on CO_2 Laser Line. Laser parameters given in Fig. 3.

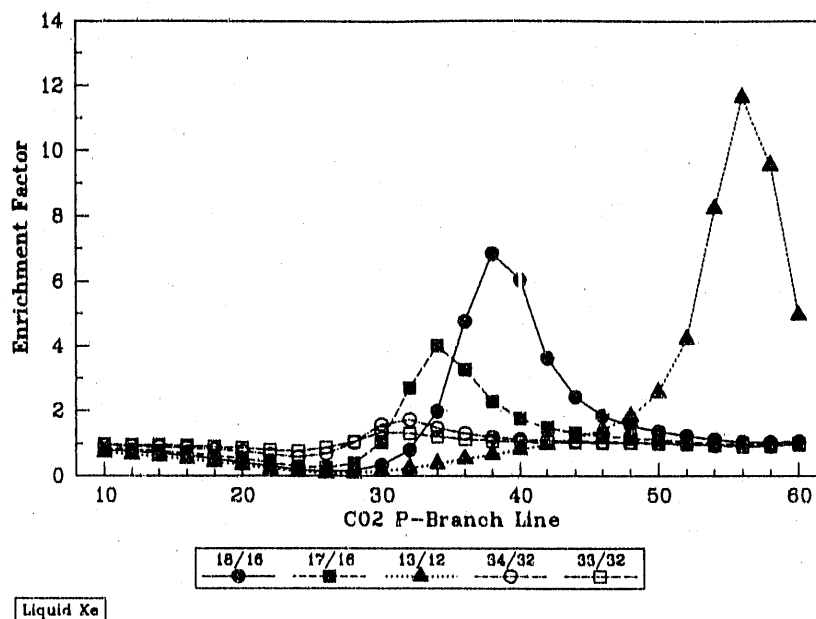
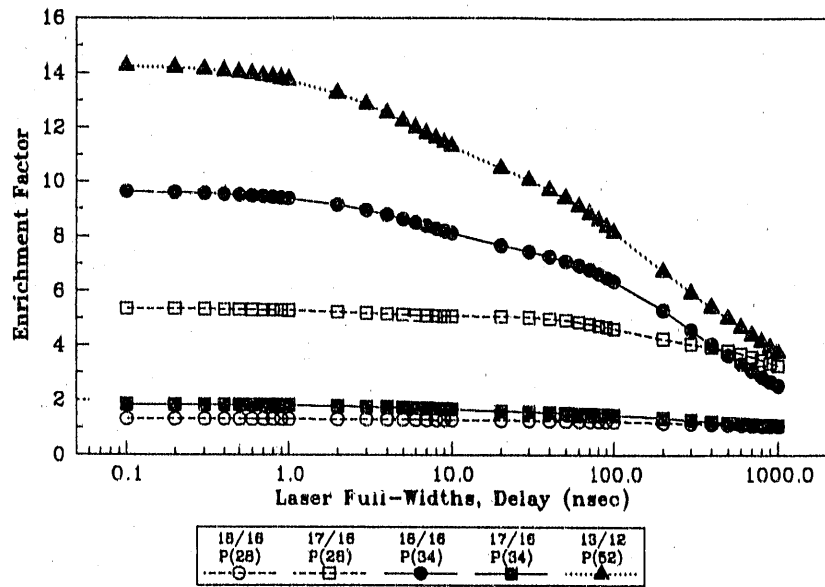


Figure 5. Dependence of Enrichment in Liquid Xe on CO₂ Laser Line. Laser parameters given in Fig. 3.

The effect of vibrational relaxation of OCS during the IR laser pumping process and during the delay between IR and UV lasers is illustrated in Fig. 6. The isotope enrichment factor is shown as a function of a characteristic two-step photodissociation time, which is the value taken identically for the laser pulse full-widths, $2\gamma_{\text{IR}}$ and $2\gamma_{\text{UV}}$, and the IR/UV delay, $\delta_{\text{IR/UV}}$. A decrease in the enrichment factor occurs on the time scale of several nanoseconds due to relaxation of the $2\nu_2$ vibrational level and on the time scale of hundreds of nanoseconds due to relaxation of the ν_1 and ν_2 levels. In order to obtain optimum enrichment factors, a photodissociation time scale of 1 to 10 ns is necessary.

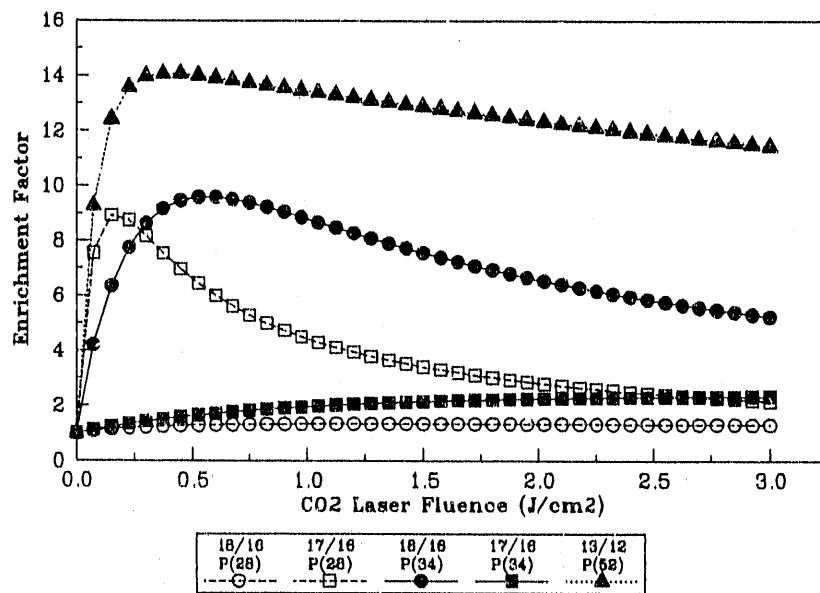
The effect of IR laser fluence (i.e., pulse energy per cm²) on the isotope enrichment factors is shown in Fig. 7. Enrichment factors are optimum where IR absorption by the selected OCS isotopomer is saturated by IR fluences of a few tenths of a Joule per cm². The enrichments decrease with higher fluences as unselected isotopomers are pumped in the wings of their absorption bands. The optimum IR laser fluence depends on band spacing and on the mismatch of the laser frequency and the selected isotopomer band center; however, the typical optimum value is approximately 0.2-0.6 J/cm². The enrichment of the "middle" isotope ¹⁷O is particularly sensitive to IR laser fluence because of overlap of the ¹⁷O absorption band with the wings of the ¹⁶O and ¹⁸O bands.

The effect of UV laser fluence on single-shot enrichment factors is illustrated in Fig. 8. The oxygen isotope enrichment factors, $\beta_{16}^0(18)$ and $\beta_{16}^0(17)$, are shown along with the dissociated fraction of isotopomers containing ¹⁸O and ¹⁷O. The decrease in enrichment with



Liquid Ar

Figure 6. Dependence of Enrichment on Laser Pulse Widths and Delay. $F_{IR}=0.75 \text{ J/cm}^2$, $F_{UV}=0.2 \text{ J/cm}^2$. Abscissa is $2\gamma_{IR}=2\gamma_{UV}=\delta_{IR/UV}$.



Liquid Ar

Figure 7. Dependence of Enrichment on CO_2 Laser Fluence. $F_{UV}=0.2 \text{ J/cm}^2$; $2\gamma_{IR}=2\gamma_{UV}=\delta_{IR/UV}=1 \text{ ns}$.

increasing UV laser fluence is due to saturation of the photodissociation out of vibrationally excited levels. In order to achieve optimum enrichments and photodissociation yields of several percent of the selected isotopomer per laser shot, UV laser fluences of several tenths of a Joule

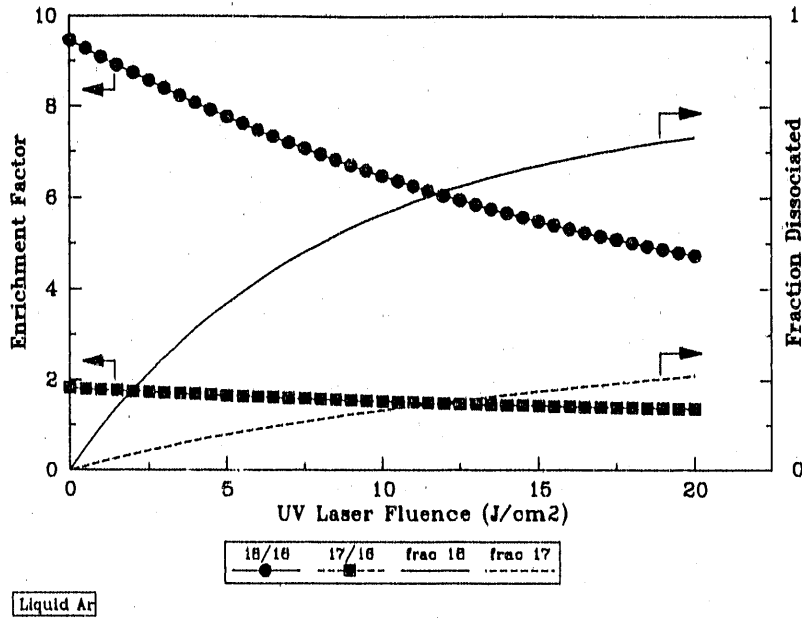


Figure 8. Dependence of Enrichment on UV Laser Fluence. $F_{IR}=0.75 \text{ J/cm}^2$; $2\gamma_{IR}=2\gamma_{UV}=\delta_{IR/UV}=1 \text{ ns}$; P(34) laser line.

per cm^2 are optimum for the vibrational levels and UV wavelength considered here.

Experimental laboratory measurements⁵ of two-step enrichments of oxygen isotopes in liquid Ar have been made using a "spike and tail" CO_2 infrared laser source with an overall pulse width substantially longer than the computer modeled optimum value. The experimental CO_2 P(32) laser pulse consisted of an initial, $\sim 100 \text{ ns}$ fwhm spike containing most of the pulse energy and a tail with an exponential decay time of $\sim 1 \mu\text{s}$. The intensity of the CO_2 laser was described approximately by Eq. (11),

$$I_{IR, \text{exptl.}}(t) = F_{IR, \text{exptl.}} \left(\frac{0.57}{\tau_{\text{spike}}} (t + \tau_{\text{spike}}) \exp \left[-\frac{t + \tau_{\text{spike}}}{\tau_{\text{spike}}} \right] + \frac{0.43}{\tau_{\text{tail}}} \exp \left[-\frac{t + \tau_{\text{spike}}}{\tau_{\text{tail}}} \right] \right) \quad (11)$$

for $t \geq -\tau_{\text{spike}}$

where $\tau_{\text{spike}}=45 \text{ ns}$, $\tau_{\text{tail}}=1 \mu\text{s}$, and $F_{IR, \text{exptl.}}=0.76 \text{ J/cm}^2$. The 249 nm, KrF excimer, UV laser used in the experiments was close to optimum with an intensity profile described by the expression for $I_{UV}(t)$ in Eq. (9) with $F_{UV}=0.24 \text{ J/cm}^2$ and $\gamma_{UV}=4 \text{ ns}$. The duration and jitter of the CO_2 laser did not allow experiments with IR/UV delay times less than $\sim 300 \text{ ns}$. A comparison of the experimental results with computer modeled enrichment factors has been discussed elsewhere⁵ and is shown in part in Fig. 9. The experimentally measured enrichment factors were the result of many laser shots and have been corrected in Fig. 9 to single-shot

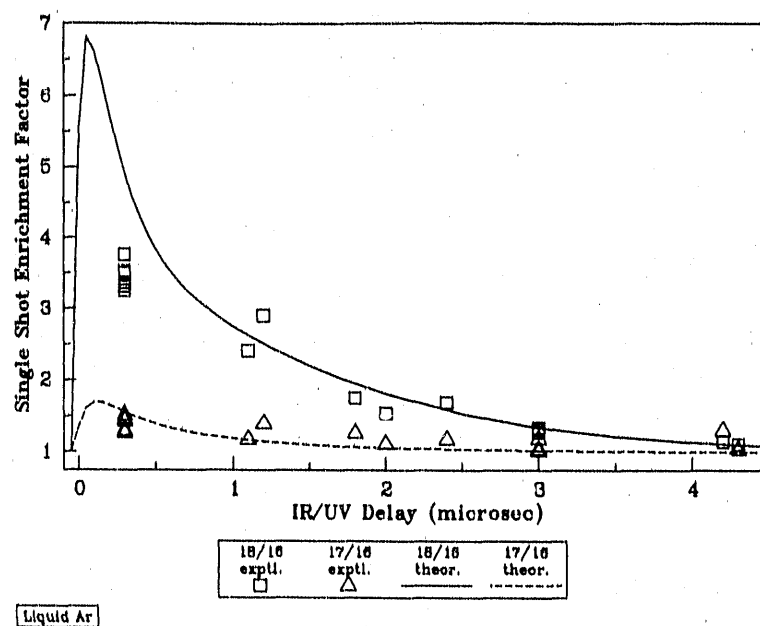


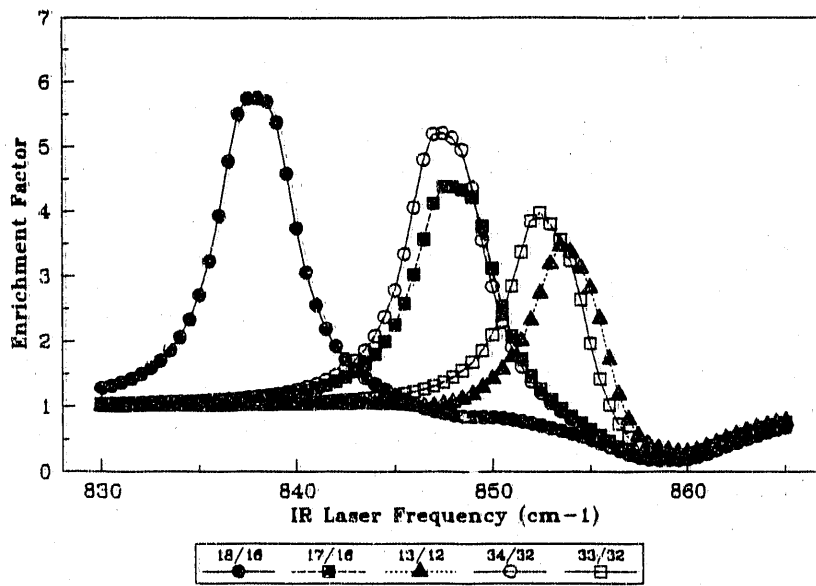
Figure 9. Comparison of Experimental and Theoretical Enrichment Factors. See text for details.

enrichments.⁵

2. Excitation in the OCS(ν_1) Band

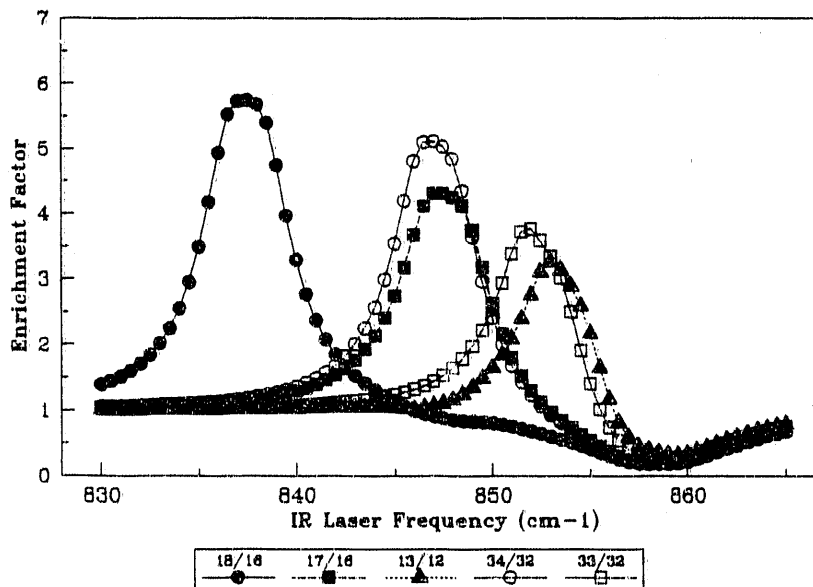
The ν_1 vibrational mode of OCS is predominantly a sulfur stretching motion and exhibits substantial isotope shifts upon sulfur isotopic substitution. A laboratory study of two-step photodissociation of room temperature, gas phase OCS through the ν_1 vibrational level has determined the 249 nm photodissociation cross section of OCS(ν_1) and has demonstrated sulfur isotope enrichments.³ No two-step photodissociation experiments through the ν_1 level have been done in cryogenic liquid solution. With the fundamental spectroscopic and vibrational relaxation data collected for cryogenically dissolved OCS, it is possible to computer model the isotope enrichments expected for two-step photodissociation through the ν_1 vibrational level in cryogenic solutions.

The kinetic equations that describe two-step photodissociation through the ν_1 vibrational level are identical to those for photodissociation through the $2\nu_2$ level (i.e., Eq. (7)) with the exception that the IR absorption terms connect the ground vibrational level with the ν_1 level instead of $2\nu_2$. Model calculations are done first for a hypothetical, tunable, short pulse, 12 μm laser source in order to determine the optimum conditions for isotope enrichment and the dependence on laser parameters. IR and UV laser intensities are described by Eq. (9). Figures 10 through 12 show isotope enrichment factors calculated for two-step photodissociation in Ar,



Liquid Ar

Figure 10. Dependence of Enrichment in Liquid Ar on 12 μm Laser Frequency. $F_{\text{IR}}=0.15 \text{ J/cm}^2$; $F_{\text{UV}}=0.2 \text{ J/cm}^2$; $2\gamma_{\text{IR}}=2\gamma_{\text{UV}}=\delta_{\text{IR/UV}}=1 \text{ ns}$.



Liquid Kr

Figure 11. Dependence of Enrichment in Liquid Kr on 12 μm Laser Frequency. Laser parameters given in Fig. 10.

Kr and Xe solutions with the nominal laser fluences, $F_{\text{IR}}=0.15 \text{ J/cm}^2$ and $F_{\text{UV}}=0.2 \text{ J/cm}^2$, and the nominal laser time characteristics, $2\gamma_{\text{IR}}=2\gamma_{\text{UV}}=\delta_{\text{IR/UV}}=1 \text{ ns}$. As in the case of the $2\nu_2$ modeling calculations, the nominal laser characteristics are chosen to ensure saturation of the

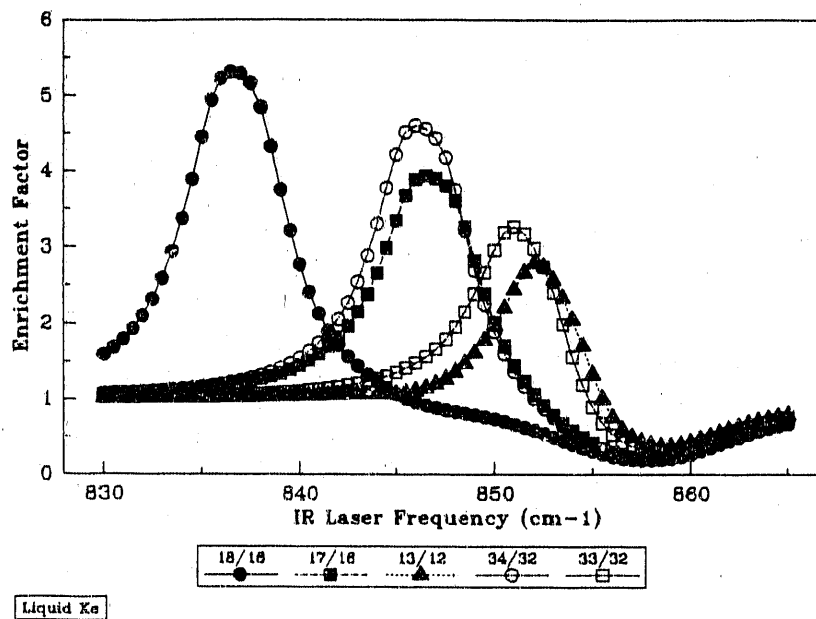


Figure 12. Dependence of Enrichment in Liquid Xe on 12 μm Laser Frequency. Laser parameters given in Fig. 10.

IR absorption step at band center, unsaturated UV photodissociation from all vibrational levels, and a time scale for the photodissociation process that is fast relative to vibrational relaxation. The isotopic band center shift for the ν_1 mode is largest ($\sim 21 \text{ cm}^{-1}$) for ^{18}O isotopic substitution. The maximum enrichment factor for ^{18}O is close to the theoretical maximum of 6.0, calculated from an expression for photodissociation through the ν_1 level that is analogous to Eq. (10). Enrichments of other isotopes are smaller because of smaller isotope shifts and consequently less than perfect isotopic resolution of the IR absorption bands.

The effect of vibrational relaxation on enrichment factors is illustrated in Fig. 13. The sulfur isotope enrichment factors obtained in liquid Ar and Kr with an IR laser pumping frequency of 847 cm^{-1} are shown as a function of a characteristic two-step photodissociation time, defined by taking $2\gamma_{\text{IR}} = 2\gamma_{\text{UV}} = \delta_{\text{IR/UV}}$. No decrease in the enrichment factors occurs for photodissociation time scales comparable to the time scale for relaxation of the $2\nu_2$ vibrational level ($\sim 10 \text{ ns}$) since the $2\nu_2$ level is never significantly populated. Enrichment initially increases with increasing photodissociation time as vibration-to-vibration ($\text{V} \rightarrow \text{V}$) relaxation is allowed to fill the ν_2 level from the laser-pumped ν_1 level, even as the ν_1 level remains saturated by the IR laser. Enrichment decreases for longer photodissociation times as both the ν_1 and ν_2 levels are vibrationally relaxed to the ground level more rapidly than they are pumped by the IR laser. In order to obtain optimum enrichment factors, a two-step photodissociation time scale of approximately 20-100 ns is necessary.

The effect of IR laser fluence on the isotope enrichment factors is shown in Fig. 14.

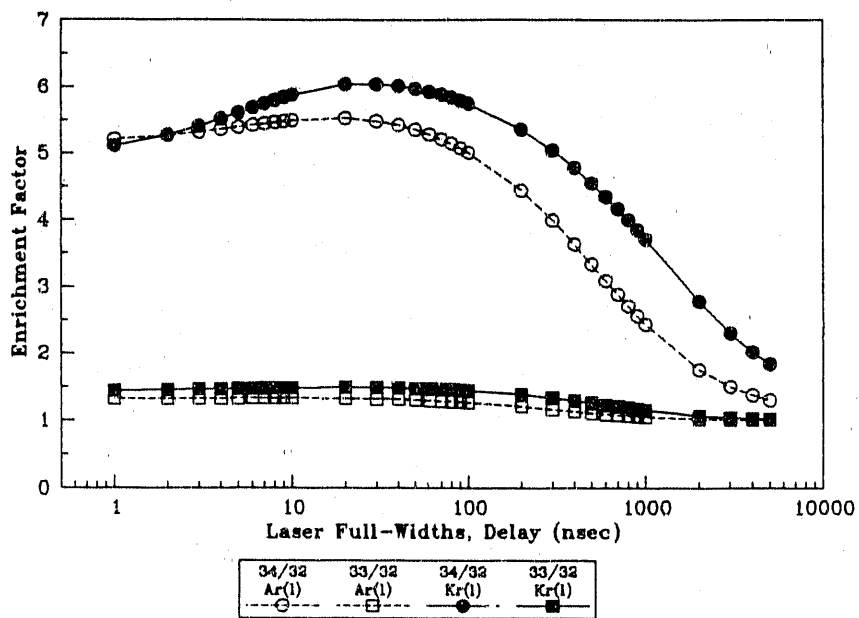


Figure 13. Dependence of Sulfur Enrichment on Laser Pulse Widths and Delay. $F_{IR}=0.15$ J/cm^2 ; $F_{UV}=0.2$ J/cm^2 . Abscissa is $2\gamma_{IR}=2\gamma_{UV}=\delta_{IR/UV}$.

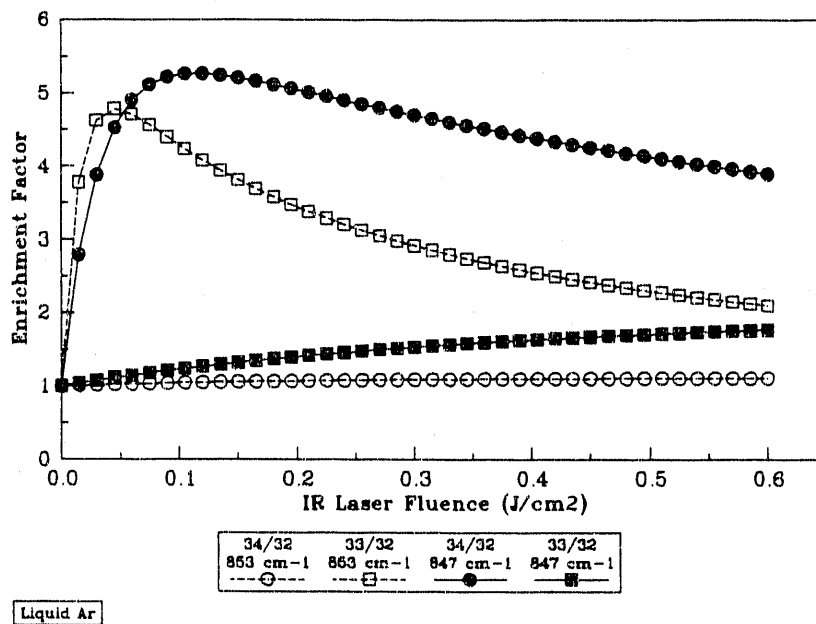


Figure 14. Dependence of Enrichment on 12 μm Laser Fluence. $F_{UV}=0.2$ J/cm^2 ; $2\gamma_{IR}=2\gamma_{UV}=\delta_{IR/UV}=1$ ns.

Saturation of a selected isotopic IR absorption band and optimum enrichments are achieved with IR laser fluences of approximately 0.05-0.15 J/cm^2 . Higher fluences disproportionately pump unselected isotomers in the wings of their absorption bands. The enrichment of the "middle"

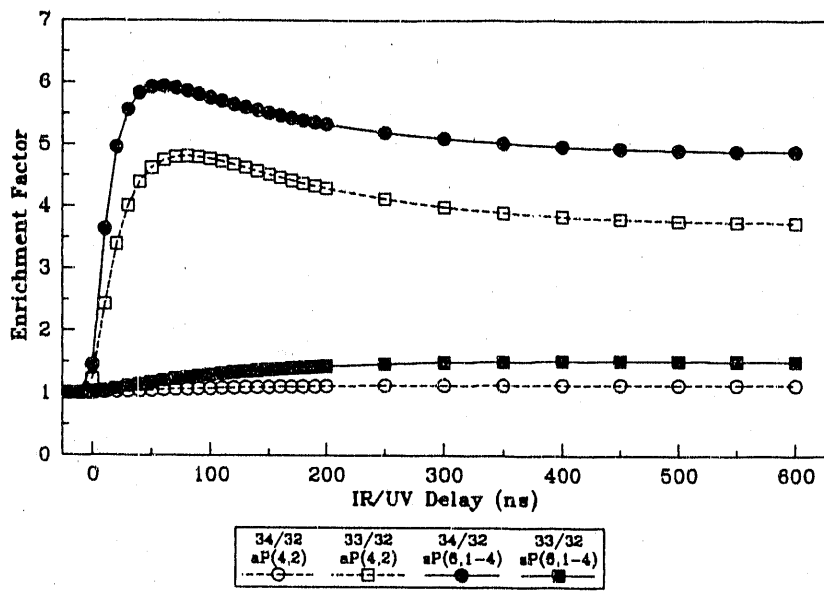
isotope ^{33}S is particularly sensitive to IR laser fluence because of overlap with the wings of the ^{32}S and ^{34}S absorption bands.

The ν_1 vibrational absorption band of OCS falls in the region of the emission lines of the NH_3 molecular laser. A CO_2 laser-pumped, NH_3 laser has been characterized and used in our laboratory to investigate two-step photodissociation of OCS in the room temperature gas phase.³ Using the characteristics of the laboratory NH_3 laser, it is possible to model with reasonably high confidence the sulfur isotope enrichment factors that could be achieved with existing NH_3 and KrF lasers. The intensity profile of the laboratory NH_3 laser is described by Eq. (12),

$$I_{IR, \text{NH}_3}(t) = F_{IR, \text{NH}_3} \frac{1}{\tau_{decay}} \exp\left[-\frac{t}{\tau_{decay}}\right] \quad (12)$$

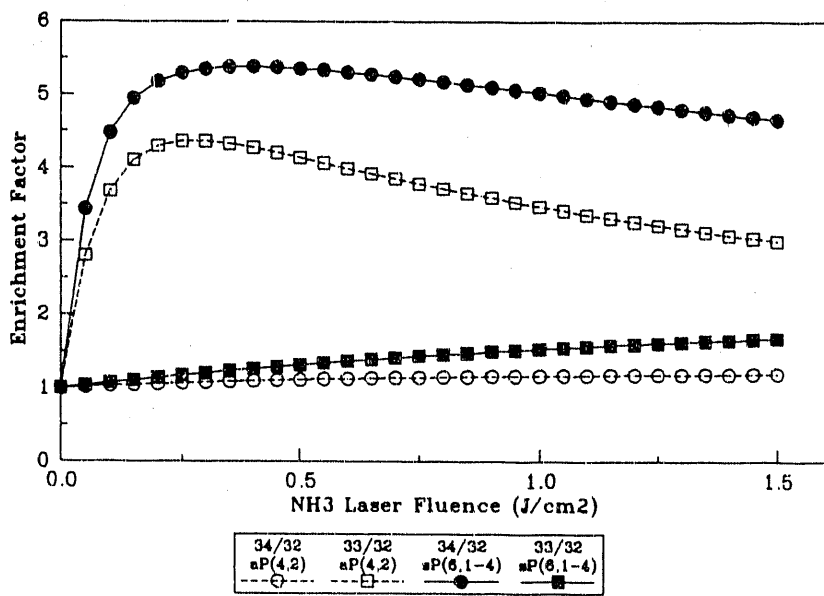
for $t \geq 0$

where $\tau_{decay} = 0.8 \mu\text{s}$. The NH_3 laser emission lines particularly relevant to sulfur isotope separation are the aP(4,2) line at 852.72 cm^{-1} and the unresolved sP(6,K=1-4) lines at an average wavenumber of 847.64 cm^{-1} . The laboratory laser produces a fluence of 0.6 J/cm^2 on the aP(4,2) line and a fluence of 0.9 J/cm^2 spread over the sP(6,K=1-4) lines in a spot of $\sim 1/2 \text{ cm}$ diameter. The UV laser used in the modeling calculations is the standard laboratory KrF excimer laser described by the expression for $I_{UV}(t)$ in Eq. (9) with $F_{UV} = 0.24 \text{ J/cm}^2$ and $\gamma_{UV} = 4 \text{ ns}$. For these laser characteristics, the enrichments of ^{33}S and ^{34}S are calculated for two-step photodissociation of OCS in liquid Ar. The enrichment factors are shown in Fig. 15 as a function of the delay between the sharp leading edge of the IR laser pulse and the center of the UV pulse. Enrichment factors calculated similarly for Kr solutions are $\sim 10\%$ larger at maximum and are optimized at slightly longer IR/UV delays. The dependence of sulfur enrichment factors on NH_3 laser fluence is shown in Fig. 16 for an IR/UV delay of 300 ns, which would be characteristic of the present laser system. The enrichments are optimum at NH_3 laser fluences of $0.2\text{-}0.4 \text{ J/cm}^2$, roughly equal to the pulse energy of the laboratory laser spread over a 1 cm diameter spot. For these experimentally realistic laser fluences and delays, the existing NH_3 and KrF lasers are found to produce sulfur isotope enrichment factors that are nearly as large as those for the hypothetical, optimized laser sources.



Liquid Ar

Figure 15. Dependence of Sulfur Enrichment on NH_3/KrF Laser Delay. See text for other laser parameters.



Liquid Ar

Figure 16. Dependence of Sulfur Enrichment on NH_3 Laser Fluence. See text for other laser parameters.

B. CONTINUOUS WAVE LASERS

The rapid vibrational relaxation of OCS by a cryogenic solvent makes it possible to maintain a *static*, non-equilibrium, isotopically enriched population of vibrationally excited OCS molecules by intense, continuous wave, IR laser radiation. A cw IR laser with an intensity of $\sim 1 \text{ MW/cm}^2$ tuned to the absorption of a particular isotopomer of OCS will maintain a constant, large population in the excited vibrational levels of the isotopomer. For small concentrations of OCS in the cryogenic solvent ($\sim 1 \text{ ppm}$), the rate of vibrational relaxation of an isotopomer to the ground vibrational level by the solvent is more rapid than the exchange of vibrational excitation among OCS isotopomers. Thus, vibrational excitation is confined primarily to the IR laser-pumped isotopomer. If the sample is simultaneously irradiated with a cw UV laser, the photodissociation products are enriched in the isotopes comprising the IR laser-pumped isotopomer.

The fundamental photophysical data obtained for OCS in cryogenic solvents can be used to computer model the isotope enrichments that would be obtained in a hypothetical, cw laser, enrichment apparatus. The kinetic equations describing the cw system are given by Eq. (7) for excitation in the $0 \rightarrow 2\nu_2$ vibrational band. The laser intensities I_{IR} and I_{UV} are constant and begin at $t=0$. The intensity of the UV laser is taken to be low enough so that the photodissociation rate out of any vibrational level of OCS is much slower than the rate at which the IR laser establishes the static, non-equilibrium population of vibrational levels (i.e., $I_{\text{UV}}\sigma_{\text{UV},2\nu_2} \ll K_{\nu_2,M}$, or roughly $I_{\text{UV}} \leq 1 \text{ MW/cm}^2$). The numerical integration of Eq. (7) is continued for the time necessary to photodissociate a few percent of the selected isotopomer. The calculated isotope enrichment factors are therefore analogous to the single-shot enrichments calculated for a pulsed laser system. The results model a practical apparatus where the UV laser intensity *and* the exposure time of the sample are adjusted to photodissociate only a small fraction of the selected OCS isotopomer.

Isotope enrichment factors for two-step, cw laser photodissociation of OCS in liquid Ar are shown in Figs. 17 and 18. In Fig. 17 the IR laser source is a line-tuned, cw CO_2 laser that pumps the $0 \rightarrow 2\nu_2$ vibrational band of OCS. The UV laser is a low intensity, 249 nm, cw source. Enrichment factors are shown as a function of CO_2 laser intensity for those laser lines that enrich ^{17}O , ^{18}O and ^{13}C isotopes. Optimum enrichments are found for a cw CO_2 laser intensity of $0.5\text{-}1.5 \text{ MW/cm}^2$. Analogous results are shown in Fig. 18 for IR excitation in the $0 \rightarrow \nu_1$ vibrational band of OCS by a hypothetical, tunable $12 \mu\text{m}$ laser. Enrichment factors are shown for ^{33}S and ^{34}S , using the optimum IR laser frequencies of 853 and 847 cm^{-1} , respectively. The optimum cw laser intensity is found to be $0.25\text{-}0.75 \text{ MW/cm}^2$. The dependence of the enrichment factors on IR laser intensity is straightforward. The enrichments peak at an IR laser intensity that is large enough to saturate the IR absorption step on the time

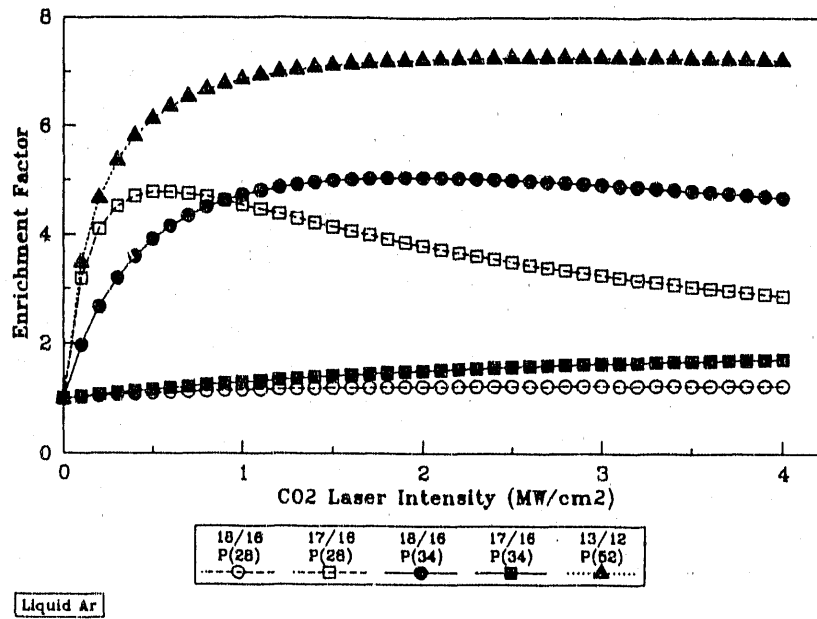


Figure 17. Dependence of Enrichment on CW, CO₂ Laser Intensity.

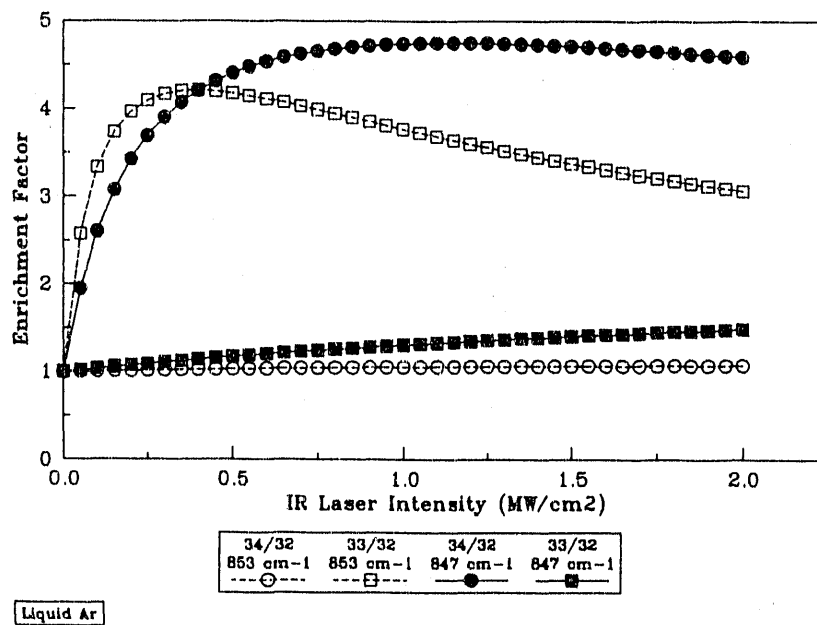


Figure 18. Dependence of Enrichment on CW, 12 μm Laser Intensity.

scale of the slowest vibrational relaxation process (i.e., roughly 1 μs). For higher IR intensities, little improvement in the pumping efficiency of the selected isotopomer is achieved; however, unselected isotopomers continue to be pumped in the low intensity wings of their absorption bands resulting in less isotopic selectivity.

A schematic example of a cw laser enrichment apparatus simulated by the computer

modeling results is shown in Fig. 19. The UV laser intensity, the length of the irradiation zone, and the liquid flow speed are chosen to generate photodissociation yields of several percent of the selected OCS isotopomer. The dimensions of the irradiation zone that are perpendicular to the flow direction may be scaled to an arbitrary size.

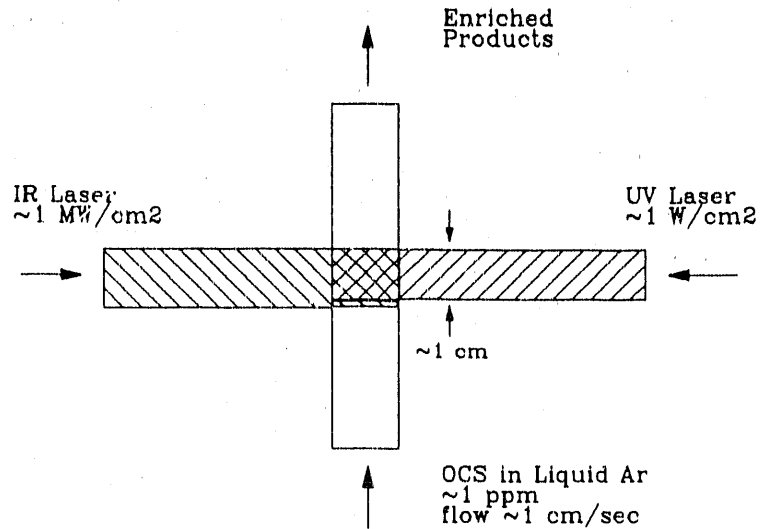


Figure 19. Schematic CW Laser Enrichment Apparatus.

IV. DISCUSSION

The computer modeling calculations define optimum laser characteristics for enriching isotopes by two-step, laser photodissociation of OCS in rare gas liquid solutions. The model calculations are based on experimentally measured optical and kinetic parameters. The only significant parameter that must be estimated is the rate of vibrational relaxation of the OCS($2\nu_2$) vibrational level, which is extrapolated from room temperature, gas phase measurements.

Two-step photodissociation through the OCS($2\nu_2$) intermediate vibrational level with pulsed lasers is found to produce optimum enrichment factors of 9-14 for ^{17}O , ^{18}O , and ^{13}C isotopes. Optimum enrichments require a line-tuned, CO_2 laser that produces a fluence of 0.2-0.6 J/cm² (e.g., a pulse energy of 0.2-0.6 Joules collimated to a 1 cm² irradiated area). The optimum pulse half-width and maximum jitter in pulse timing are in the range of 1-10 ns. The temporal requirements on the laser pulses are determined primarily by the $2\nu_2$ vibrational level relaxation time. The CO_2 laser requirements are only slightly beyond those of commercially available systems and are within the reach of specially designed oscillator/amplifier systems. The characteristics of the optimum KrF laser source are a fluence of several tenths of a Joule per cm² and a pulse half-width of 1-10 ns with comparable timing jitter. The UV pulse is delayed from the IR pulse by approximately the sum of the IR and UV pulse half-widths. The characteristics of the optimum KrF laser are available in commercial excimer lasers. Enrichments measured in recent laboratory experiments have been limited by CO_2 laser pulse duration and jitter to approximately a factor of 3 less than optimum.

Pulsed, IR/UV photodissociation through the OCS(ν_1) intermediate vibrational level is found to produce optimum enrichment factors of 5-6 for ^{33}S and ^{34}S isotopes. The optimum IR laser source is a tunable 12 μm laser, producing a fluence of 0.05-0.15 J/cm² with a pulse half-width of 20-100 ns. The optimum temporal characteristics of the lasers are determined primarily by the vibrational relaxation times of the ν_1 and ν_2 vibrational levels. The optimum KrF excimer laser is essentially the same as for photodissociation through the $2\nu_2$ level, although the requirement on pulse half-width may be relaxed to 20-100 ns. The totally optimized 12 μm laser source is hypothetical and not yet commercially available; however, nearly optimum enrichment factors can be achieved using a real, NH_3 molecular laser as the IR source. The approximate characteristics of the NH_3 laser are a fluence of 0.2-0.4 J/cm² on the aP(4,2) emission line, or spread over the sP(6,K=1-4) emission lines, and a pulse full-width of $\sim 1/2$ μs .

Enrichment factors have been modeled in liquid Ar, Kr, and Xe. The optimum enrichments found in liquid Kr and Xe are not significantly different from those found in the more practical liquid Ar solvent. Slower vibrational relaxation times in liquid Kr and Xe allow optimum laser pulse widths and delays to be slightly longer; however, the wider vibrational

absorption bandwidths lead to slightly smaller optimum enrichment factors. For a real isotope enrichment apparatus, an inexpensive solvent such as liquid nitrogen is most practical. No fundamental optical, or kinetic, data are available for modeling enrichments in liquid nitrogen. It is likely that vibrational absorption bandwidths in liquid nitrogen are not much different from those in liquid Ar. Extrapolating from sparse, room temperature data for the vibrational relaxation of OCS by Ar and N₂ (and the similar molecule CO),⁷⁻¹⁰ it seems likely that OCS vibrational relaxation times in liquid N₂ are roughly a factor of 3-10 faster than in liquid Ar. Thus, optimum enrichments in liquid N₂ may be similar to those in the liquid rare gases; however, the optimum laser pulse widths and IR/UV delays would probably be a factor of 3-10 shorter.

The optimum isotope enrichment factors modeled for continuous wave laser photodissociation of OCS in cryogenic liquids are smaller than those found for pulsed lasers. The power requirement for the CO₂, or 12 μm, IR laser source is on the order of 1 MW/cm². The extremely high power requirement and the photon inefficiency of maintaining a non-equilibrium vibrational population distribution for times that are long compared to vibrational relaxation times are unattractive features of the cw enrichment scheme. In principle, photon efficiency could be improved by increasing the cw UV laser intensity to the megawatt level and reducing sample exposure times to microseconds; however, these modifications do not seem practical. Although a continuous flow enrichment system may be generally desirable for simplicity of operation and high throughput, it is not a good system for isotopically selective, two-step photodissociation of OCS. Higher enrichments and higher photon efficiencies are achieved with pulsed laser sources.

INTERNAL DISTRIBUTION LIST

REPORT TITLE **A COMPUTER MODELING STUDY OF ISOTOPICALLY SELECTIVE, LASER PHOTODISSOCIATION OF OCS IN CRYOGENIC SOLUTIONS**

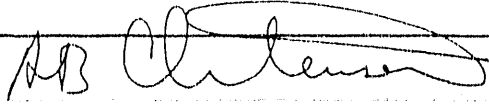
REPORT NO. **ATR-91(7171)-2** PUBLICATION DATE **23 December 1991** SECURITY CLASSIFICATION **Unclassified**

1. FOR OFF-SITE PERSONNEL, SHOW LOCATION SYMBOL.
e.g., JOHN O. PUBLIC/VAFB

2. IF LIST IS ALTERED, INITIAL CHANGE(S) AND SHOW AFFILIATION
* FOR SECRET REPORTS SHOW BLDG AND ROOM, NOT MAIL STATION

<u>NAME (Include Initials)</u>	<u>MAIL CODE *</u>
J. B. Blake	M2/259
A. B. Christensen (2)	M2/254
D. J. Evans	M2/264
J. F. Fennell	M2/259
J. R. Hallet	M2/278
C. K. Howey	M2/255
D. J. Gorney	M2/255
H. C. Koons	M2/260
V. I. Lang	M2/251
A. T. Pritt	M2/251
C. J. Rice	M2/266
H. R. Rugge	M2/264
A. J. Schiewe	M1/002
M. Schulz	M2/259
J. J. Shaffer	M2/279
R. L. Walterscheid	M2/255
P. E. Zittel (3)	M2/251

NAME (Include Initials) MAIL CODE *

APPROVED BY  DATE **2-3-92**

* IF LIST COMPRISES TWO OR MORE SHEETS, COMPLETE ABOVE BLOCK ON LAST SHEET ONLY

EXTERNAL DISTRIBUTION LIST

REPORT TITLE

A COMPUTER MODELING STUDY OF ISOTOPICALLY SELECTIVE,
LASER PHOTODISSOCIATION OF OCS IN CRYOGENIC SOLUTIONS

REPORT NO.

ATR-91(7171)-2

PUBLICATION DATE

23 December 1991

SECURITY CLASSIFICATION

Unclassified

MILITARY AND GOVERNMENT OFFICES

ASSOCIATE CONTRACTORS AND OTHERS

1. SHOW FULL MAILING ADDRESS: INCLUDE ZIP CODE, MILITARY OFFICE SYMBOL, AND "ATTENTION" LINE
2. IF LIST IS ALTERED, INITIAL CHANGE(S) AND SHOW AFFILIATION

U. S. Department of Energy
San Francisco Operations
Contracts Management Division
1333 Broadway
Oakland, CA 94612
(3 copies)

U. S. Department of Energy
Division of Chemical Sciences
Washington, DC 20545
Attn: Dr. John L. Burnett
ER-142, MS G-236, GTN

DISTRIBUTION LIMITATIONS MARKED ON THE COVER/TITLE PAGE ARE AUTHORIZED BY SIGNATURE BELOW

APPROVED BY
(AEROSPACE)



DATE

2-3-92

APPROVED BY
(AF OFFICE)

(NOT REQUIRED FOR ATR CATEGORY)

DATE

IF LIST COMPRISES TWO OR MORE SHEETS, COMPLETE ABOVE BLOCK ON LAST SHEET ONLY

SHEET

1

OF

1

**DATE
FILMED**

5/01/92

